Paper No. 39

SIMULATION OF THREE-DIMENSIONAL COOLANT FLOW WITHIN TRANSPIRATION NOSETIPS*

J. R. Schuster and G. E. Seay, *McDonnell Douglas Astronautics, Huntington Beach, California*

ABSTRACT

Steady-state equations are presented to describe coolant mass and energy transfer within transpiration nosetips. The energy model, which assumes thermal equilibrium between the coolant and matrix, is justified on the basis of pore size. An iterative computational technique is given which can be applied to the finite-difference equivalents of the steady-state equations, causing a relaxation in the pressure and enthalpy fields to satisfy the boundary conditions. To maintain stability, the calculations must be damped. The final results show isothermal approximations to be substantially in error for high- and low-pressure reentry conditions.

NOMENCLATURE

A = Interfacial area between nodes, ft^2

C_p = Specific heat, $Btu/lb_m\text{-}°R$

D = Diameter, ft

E = Energy flow into or out of a node, Btu/sec

$\dot{e}$ = Energy flux defined by Equation (26), $Btu/ft^2\text{-sec}$

f = Function defined by Equation (25)

g_c = Conversion factor, 32.17 $lb_m\text{-ft}/lb_f\text{-sec}^2$

H = Fluid enthalpy, Btu/lb_m

h = Heat-transfer coefficient, $Btu/ft^2\text{-sec-}°R$

J = Conversion factor, 778 $ft\text{-}lb_f/Btu$

*This work was supported by McDonnell Douglas independent research and development funds.

522-137 O - 73 - 35

K = Porous matrix permeability, ft^2

k = Conductivity, Btu/ft-sec-°R

L = Length measurement in direction of mass flow, ft

M = Mass flow into or out of a node, lb_m/sec

$\dot{m}$ = Effective fluid mass flux based on matrix cross section, lb_m/ft^2-sec

N = Number of pores per unit matrix cross section, ft^{-2}

P = Pressure, lb_f/ft^2

$\dot{Q}$ = Conduction heat flux, Btu/ft^2-sec

R = Porous matrix heat flow parameter defined by Equation (22), Btu/sec-°R

T = Temperature, °R

v = Effective fluid velocity based on matrix cross section, ft/sec

W = Porous matrix fluid flow parameter defined by Equation (18), sec/ft

y = Distance from outer surface of porous matrix, ft

α = Porous matrix viscous pressure drop constant, ft^{-2}

β = Porous matrix inertial pressure drop constant, ft^{-1}

Γ = Porous matrix tortuosity for heat conduction, dimensionless

γ = Porous matrix void fraction, dimensionless

μ = Fluid viscosity, lb_m/ft-sec

ρ = Fluid density, lb_m/ft^3

$\overline{\sigma}$ = Elemental surface area normal vector, ft^2

Subscripts

e = Effective value

c = Value for coolant

in = Into a node

o = Storage value

out = Out of a node

pore = Value for pore within the porous matrix

s = Value for porous matrix parent material

surf = Outer surface value

0, 1, 2, 3, 4, 5, 6 = Nodal subscripts defined by Figure 5

INTRODUCTION

The design of a transpiration-cooled nosetip, represented in the cross section in Figure 1, is predicated upon delivering coolant to the nosetip surface at a rate sufficient to dissipate thermal energy from aerodynamic heating. From this standpoint, ideal coolant flux at the surface varies greatly with location; it can be complicated by aerodynamic boundary-layer transition and angle of attack. For reentry vehicle application, it is desirable to minimize wastage of coolant, i.e., no excess coolant flux should be delivered to any portion of the nosetip surface. However, this is difficult to accomplish in view of the severe pressure gradient that can exist over the nosetip surface at high stagnation pressures. The pressure gradient acting over the surface is transmitted to the isotropic porous material of the nosetip, and when superimposed on the internal radial pressure field, it can cause significant bending of coolant streamlines between the inner and outer surfaces of the nosetip. To define coolant distribution accurately at the outer surface, three-dimensional porous flow calculations must be done because of the surface pressure gradient, coupled with the irregular shape of the nosetip inner surface and the effects of angle of attack.

LITERATURE REVIEW

The traditional approach to analyzing incompressible steady flow through porous media has been to assume the process is dominated by viscous effects and that effective fluid velocity averaged over a typical cross section is proportional to the pressure gradient and a material property called permeability. The resulting relationship, Equation (1), is sometimes referred to as the Darcy[1] equation.

$$-\frac{dP}{dL} = \frac{\mu}{Kg_c} v \qquad (1)$$

To better match experimental data, Green and Duwez[2] modified the Darcy equation by adding terms to account for inertial or nonviscous effects within the porous flow:

$$-\frac{dP}{dL} = \frac{(\alpha\mu + \beta\rho v)\, v}{g_c} \tag{2}$$

where α is the viscous pressure drop constant (the inverse of the material permeability) and β is the inertial pressure drop constant of the material. In order to characterize a specific porous material, both α and β should be evaluated experimentally, as they strongly depend on such factors as material porosity and pore shape and size.

Equation (2) can be extended to multidimensional flow in isotropic porous media provided the acceleration due to flow curvature is neglected.

$$-\nabla P = \frac{(\alpha\mu + \beta\rho|v|)\,\bar{v}}{g_c} \tag{3}$$

Considering only viscous pressure drop, Schneider and Maurer[3] utilized Equation (3) to obtain analytic solutions for the flow of coolant through a hemispherical, transpiration-cooled shell subjected to a Newtonian surface-pressure distribution. They found that with streamline curvature, there is a tendency toward coolant starvation in the stagnation region, and that one-dimensional calculations are inadequate.

In order to study other shapes besides concentric hemispheres and to include inertial effects, Timmer and Dirling[4] treated the axisymmetric porous nosetip flow problem by approximating the quantity $(\alpha\mu + \beta\rho|v|)$ as a constant for the porous region, thus reducing Equation (3) to Laplace's equation.

$$\nabla^2 P = 0 \tag{4}$$

By assuming symmetry in a plane normal to the nosetip axis, the question becomes an interior Dirichlet problem, and for a given set of boundary conditions, may be solved numerically using the method of Hess[5]. If an analytic external pressure distribution such as modified Newtonian is assumed for the outer surface, then the linearity of Laplace's equation permits the decoupling of the complex numerical calculations from the physical boundary conditions. The physical solution is then represented by summation of three separate sets of simple artificial boundary conditions.

Gold et al.[6] examined the nosetip porous flow problem for angle of attack. They reduced the flow to Laplace's equation by ignoring inertial effects and approximating the surface-pressure distribution as an analytic function of the meridian angle and the pressures on windward, yaw, and leeward meridians. They utilized nondimensional graphical data for fixed angles of attack to determine coolant distributions.

Although the previous porous flow analyses for transpiration nosetips are useful, they have several drawbacks:

1. Conservation of coolant mass is ignored inside the porous matrix.

2. Inertial effects are either approximated or ignored.

3. The nosetip analysis is restricted by the assumption of symmetry.

4. The external pressure profiles must be described as simple analytic functions.

5. The analyses assume constant coolant properties; i.e., isothermal flow.

Curry and Cox[7] developed a set of complex equations for the transient flow of a compressible gas through porous media with heat transfer. They solved some two-dimensional low-heating cases numerically. Although their method is general, the numerical techniques are extremely difficult to extend to three dimensions (for angle of attack).

This paper describes and demonstrates an analytical model and numeric technique that does not have the shortcomings of some of the previous work. The analysis

1. Is general with regard to geometry and boundary conditions.

2. Permits porous media heat transfer.

3. Is steady-state.

4. Is three-dimensional.

It is currently in use as an analytical and design tool for the development of transpiration-cooled nosetips.

ANALYSIS

The object of this analysis is to provide a steady-state solution for coolant distribution on the outer surface of a

transpiration-cooled nosetip. Because typical operating conditions may involve high stagnation pressures, the final numerical relationships should provide for variable real-fluid properties in terms of local temperature and pressure. Therefore, it is necessary to solve for the temperature distribution as well as the pressure distribution throughout the porous matrix.

Basic Equations

The basic equation for porous-flow pressure drop is a minor modification of Equation (3):

$$- g_c \nabla P = (\alpha\mu + \beta\dot{m}) \frac{\overline{\dot{m}}}{\rho} \tag{5}$$

where the velocity vector has been replaced by the mass flux vector, $\overline{\dot{m}}$.

In addition, there is the steady-state continuity equation

$$\oint_s (\overline{\dot{m}}) \cdot d\overline{\sigma} = 0 \tag{6}$$

and the steady-state porous-flow energy equation

$$-k_e \nabla^2 T - (\nabla k_e) \cdot (\nabla T) + \nabla \cdot (H\overline{\dot{m}}) = 0 \tag{7}$$

The local effective thermal conductivity is that of the coolant-infiltrated matrix, and is determined by the following equation

$$k_e = \gamma k_c + (1-\Gamma)(1-\gamma) k_s \tag{8}$$

where

k_c = the local coolant conductivity

k_s = local conductivity of porous matrix parent material

γ = void fraction of porous matrix

Γ = porous matrix tortuosity

Assessment of Thermal Equilibrium

Equation (7) assumes that the fluid within a pore and the surrounding pore material are in thermal equilibrium. This assumption can be examined by the following approximations. Figure 2 presents an idealized one-dimensional flow through a matrix composed of circular pores. Assuming thermal equilibrium and uniform conductivity, Equation (7) reduces to

$$\dot{Q} = -k_e \frac{dT}{dy} = \dot{m}(H_c - H_{c,o}) \tag{9}$$

where $H_{c,o}$ is the coolant storage enthalpy.

Examining the energy exchange within the pores, a balance yields

$$-\dot{m} C_{p_c} \frac{dT}{dy} = N\pi D_{pore} \dot{Q}_{pore} \tag{10}$$

while the pore density per unit area is

$$N = \frac{4\gamma}{\pi D_{pore}^2} \tag{11}$$

Within a pore, the porous matrix-to-coolant temperature differential is

$$T_s - T_c = \frac{\dot{Q}_{pore}}{h_{pore}} \tag{12}$$

Assuming purely laminar flow within a pore, the pore heat-transfer coefficient is

$$h_{pore} \simeq \frac{4\, k_c}{D_{pore}} \tag{13}$$

Combining Equations (9) through (13), the porous matrix-to-coolant temperature differential is

$$T_s - T_c = 0.0625\, D_{pore}^2\, \dot{m}^2 \frac{C_{p_c}}{\gamma k_c k_e} (H_c - H_{c,o}) \tag{14}$$

Approximating $(H_c - H_{c,o})$ as $C_{p_c}(T - T_{c,o})$, Equation (9) can be integrated and combined with Equation (14) to yield the local temperature differential in terms of the total enthalpy rise of the coolant at the surface (a function of the surface pressure) and the distance from the surface.

$$T_s - T_c = 0.0625\, D_{pore}^2\, \dot{m}^2 \frac{C_{p_c}}{\gamma k_c k_e}\left(H_{c,surf} - H_{c,o}\right) \exp\left(-\frac{\dot{m}\, C_{p_c}}{k_e} y\right) \tag{15}$$

Equation (15) indicates that the maximum temperature differential will occur at the surface where the coolant enthalpy is a maximum, and that the differential will decrease in exponential fashion below the surface.

As transpiration nosetip materials consist of sintered metallic powders of various particle sizes, it is necessary to characterize the pore distribution in order to assess the degree of thermal inequilibrium. Figure 3 presents a pore size distribution, based on mercury-intrusion porosimeter tests, for a typical sintered stainless-steel nosetip material with a porosity of 20.3 percent. The median pore size is 2.7 microns. For a typical mass flux of liquid water of 20 lb_m/ft^2-sec at a surface pressure of 200 atm, saturated liquid conditions on the surface result in a porous matrix-to-coolant temperature differential of 50°F. This decreases to 5°F 0.002 in. below the surface. It can be readily seen that thermal equilibrium is a good assumption for coolant flow within the porous matrix.

Viscous Dissipation

If a liquid coolant is caused to flow through a nosetip by an imposed pressure differential, the coolant temperature will rise because frictional shear forces transform the flow work done on the coolant into thermal energy (i.e., viscous dissipation). If the coolant flow is assumed to be adiabatic, the local temperature of the incompressible fluid in the porous matrix is

$$T_c = T_{c,o} + \frac{P_{c,o} - P_c}{\rho C_{p_c} J} \tag{16}$$

where J is the mechanical equivalent of heat. For water, this temperature change amounts to about 3 °F for each 1,000-psi differential in pressure. In reality, the flow process is not adiabatic, the coolant is not incompressible, and some kinetic energy is imparted to the coolant. However, for water, the latter two effects are negligible. Additionally, if the flow rate is high enough to negate the effect of heat conduction along coolant flow vectors within the porous matrix, as indicated by Equation (9), then the assumption of adiabatic flow is appropriate. Since liquid viscosity is usually a strong function of temperature, viscous dissipation can have a significant effect on coolant pressure drop and flow distribution.

FINITE-DIFFERENCE MODELING

The porous transpiration nosetip is segmented radially, axially, and circumferentially so as to form a nodal network, as illustrated in Figure 4. The interfacial areas bordering nodes and the distances between centroids of adjacent nodes are evaluated and utilized in conjunction with Equations (5) through (7) to determine pressures and temperatures at node centroids and the mass and energy flow either into or out of each nodal face. To satisfy Equation (6), the interfacial areas between nodes are corrected for nonorthogonality by multiplying them by the unit vector dot product between the normal to the face and the line connecting the centroids of the adjacent nodes. Due to symmetry about the plane passing through the windward and leeward meridians, only half the nosetip need be analyzed. Using the numbering system of Figure 5, the finite-difference, Cartesian equivalent of Equation (5) is

$$\dot{m}_{0,4} = g_c W_{0,4} (P_0 - P_4)$$

$$\dot{m}_{0,5} = g_c W_{0,5} (P_0 - P_5) \qquad (17)$$

$$\dot{m}_{0,6} = g_c W_{0,6} (P_0 - P_6)$$

where

$$W_{0,4} = \frac{2}{L_{0,4}\left[\frac{\alpha\mu_0 + \beta\dot{m}_0}{\rho_0} + \frac{\alpha\mu_4 + \beta\dot{m}_4}{\rho_4}\right]}$$

$$W_{0,5} = \frac{2}{L_{0,5}\left[\frac{\alpha\mu_0 + \beta\dot{m}_0}{\rho_0} + \frac{\alpha\mu_5 + \beta\dot{m}_5}{\rho_5}\right]}$$

$$W_{0,6} = \frac{2}{L_{0,6}\left[\frac{\alpha\mu_0 + \beta\dot{m}_0}{\rho_0} + \frac{\alpha\mu_6 + \beta\dot{m}_6}{\rho_6}\right]} \qquad (18)$$

The equivalent of Equation (6) is

$$\dot{m}_{1,0}A_{1,0} + \dot{m}_{2,0}A_{2,0} + \dot{m}_{3,0}A_{3,0} = M_{in}$$

$$= M_{out} = \dot{m}_{0,4}A_{0,4} + \dot{m}_{0,5}A_{0,5} + \dot{m}_{0,6}A_{0,6} \qquad (19)$$

Substituting Equation (17) into Equation (19) and rearranging,

$$P_0 = \frac{\frac{M_{in}}{g_c} + \left[W_{0,4}A_{0,4}P_4 + W_{0,5}A_{0,5}P_5 + W_{0,6}A_{0,6}P_6\right]}{\left[W_{0,4}A_{0,4} + W_{0,5}A_{0,5} + W_{0,6}A_{0,6}\right]} \qquad (20)$$

Equation (20) presents a relationship for the nodal pressure in terms of the net mass flow-in from three adjacent nodes and the pressures in and geometric relationships with the other three adjacent nodes.

The energy relationship, Equation (7), becomes

$$E_{in} = \dot{m}_{1,0}H_1A_{1,0} + \dot{m}_{2,0}H_2A_{2,0} + \dot{m}_{3,0}H_3A_{3,0}$$

$$+ R_{1,0}(T_1-T_0) + R_{2,0}(T_2-T_0) + R_{3,0}(T_3-T_0)$$

$$= E_{out} = \dot{m}_{0,4}H_0A_{0,4} + \dot{m}_{0,5}H_0A_{0,5} + \dot{m}_{0,6}H_0A_{0,6} \qquad (21)$$

$$+ R_{0,4}(T_0-T_4) + R_{0,5}(T_0-T_5) + R_{0,6}(T_0-T_6)$$

where

$$R_{0,4} = 0.5\frac{A_{0,4}}{L_{0,4}}\left(k_{e_0} + k_{e_4}\right)$$

$$R_{0,5} = 0.5\frac{A_{0,5}}{L_{0,5}}\left(k_{e_0} + k_{e_5}\right) \tag{22}$$

$$R_{0,6} = 0.5\frac{A_{0,6}}{L_{0,6}}\left(k_{e_0} + k_{e_6}\right)$$

Equation (21) can be rearranged to two forms:

$$T_0 = \left(E_{in} - \dot{m}_{0,4}H_0A_{0,4} - \dot{m}_{0,5}H_0A_{0,5} - \dot{m}_{0,6}H_0A_{0,6} + R_{0,4}T_4 + R_{0,5}T_5 + R_{0,6}T_6\right)\Big/\left(R_{0,4} + R_{0,5} + R_{0,6}\right) \tag{23}$$

or

$$H_0 = \frac{E_{in} - R_{0,4}(T_0 - T_4) - R_{0,5}(T_0 - T_5) - R_{0,6}(T_0 - T_6)}{\dot{m}_{0,4}A_{0,4} + \dot{m}_{0,5}A_{0,5} + \dot{m}_{0,6}A_{0,6}} \tag{24}$$

where

$$H_0 = f(T_0, P_0) \tag{25}$$

Equation (24) is used in the present analysis as it provides greater stability in the numerical solution.

The Cartesian energy fluxes are

$$\dot{e}_{0,4} = \dot{m}_{0,4}H_0 + \frac{R_{0,4}}{A_{0,4}}(T_0 - T_4)$$

$$\dot{e}_{0,5} = \dot{m}_{0,5}H_0 + \frac{R_{0,5}}{A_{0,5}}(T_0 - T_5)$$

$$\dot{e}_{0,6} = \dot{m}_{0,6} H_0 + \frac{R_{0,6}}{A_{0,6}} (T_0 - T_6) \tag{26}$$

Boundary Conditions

As the inner and outer surfaces of the nosetip are represented by dummy nodes, essentially any prescribed distributions of pressure, mass flux, temperature, or heat flux can be simulated. Practical cases involve the following set of conditions:

1. Specified constant pressure over the inner surface of the nosetip.

2. Specified constant coolant-supply temperature (permits heat conduction at the inner surface of the nosetip).

3. Specified pressure distribution over the outer surface of the nosetip.

4. Local saturation temperature over the outer surface corresponding to the prescribed pressure distribution.

The fourth boundary condition is justified for liquids because the surface shear encountered during reentry drastically reduces the coolant flow within the surface film by causing liquid to be stripped from the film and entrained in the gaseous boundary layer.[8] In proportion, this reduces the film thickness, and allows the porous matrix surface to approach the local vaporization temperature of the coolant. This interpretation is supported by recent experimental data indicating surface temperature essentially equal to the vaporization temperature in regions covered by a liquid film.

Iteration Technique

Initial estimates of the pressure, mass flux, and temperature and energy flux distributions are made within the nodal matrix representing the nosetip. The mass and energy flow from the nosetip cavity into the innermost node bordering the nosetip axis of symmetry and centered on the windward meridian is then calculated utilizing Equations (17) and (26). This provides an updated value for mass flow into that node; therefore, an updated nodal pressure and temperature can be calculated using Equations (20) and (24). With the updated pressure and temperature, Equations (17) and (26) can then be utilized to evaluate updated mass fluxes and energy fluxes from that node into the three adjacent nodes in the outward radial direction,

the downstream axial direction, and the circumferential direction toward the leeward meridian.

This technique is then applied to successive nodes radially and outward until the surface is reached, whereupon a transfer is made to the innermost node in the adjacent row in the downstream axial direction. After a pass has been made through the row of nodes furthest downstream, a transfer is then made to the adjacent bank of nodes in the circumferential direction and the sequence is repeated.

The basis for the technique is that the fixed temperature and pressure boundary conditions cause a relaxation in the matrix internal pressure and enthalpy and temperature distributions until conservation of coolant mass and energy is achieved. Convergence is obtained when each nodal pressure and enthalpy varies by less than a specified percentage from the value on the previous pass through the network; i.e., for the i^{th} iteration, $(P_{0,i} - P_{0,i-1})/(P_{0,i-1}) <$ convergence margin and $(H_{0,i} - H_{0,i-1})/(H_{0,i-1}) <$ convergence margin.

To maintain a uniform progression from the initialized distributions to the final solution, the calculations must be damped by weighting the updated nodal pressure and enthalpy as determined by Equations (20) and (24) with the values on the previous pass; i.e.,

$$P_{0,i} = \text{damping factor} \times P_{0,\text{calculated}} + (1.0\text{-damping factor}) \times P_{0,i-1}$$

and (27)

$$H_{0,i} = \text{damping factor} \times H_{0,\text{calculated}} + (1.0\text{-damping factor}) \times P_{0,i-1}$$

where a decreasing damping factor results in increased damping.

If the damping is inadequate, oscillations result in the internal pressure and enthalpy fields, either slowing convergence or causing the calculations to become unstable. The amount of damping required appears to increase with both the number of nodes in the mesh representing the nosetip and the

variation between the initially estimated and final pressure and enthalpy distributions. Subsequent numerical results that will be shown utilize one-dimensional estimates for the initial distributions. It has also been determined that as the amount of damping and number of nodes in the mesh increase, the convergence margin must be decreased to maintain accuracy.

RESULTS

For the nosetip contour shown in Figure 1, with a radius of 1.0 in., a series of calculations was performed to determine the material permeability that most efficiently distributed the coolant around the nosetip surface. The optimum permeability was found to be 5.45×10^{-11} in.^{2}. Utilizing this permeability and some typical reentry conditions, studies and comparisons were made utilizing a computerized model of the analyses. Surface pressure distributions were obtained from a method-of-characteristics solution of the inviscid shock layer.

Critical Parameter Requirements

Isothermal porous flow and 0-deg angle of attack were selected in order to study the damping and convergence requirements and the relative accuracy obtained by varying the fineness of the nosetip mesh. Figure 6 gives an approximate indication of the amount of damping required to obtain convergence as a function of mesh dimensions. Above the curve, the calculations tend to go unstable. As the curve is approached from below, the oscillations take longer to damp out. Rapid convergence is usually obtained with the damping factor set about 10 percent below the critical value.

Since one-dimensional relationships are used to establish the initial estimates of pressure and enthalpy field, other nosetip geometries that are not proportional may require damping other than that shown in Figure 1. However, the trend with increasing mesh fineness should hold. Multiplying the total number of nodes by circumferentially segmenting the nosetip to simulate angle of attack seems to have little or no effect on the damping requirement. The radial and axial mesh fineness are the primary factors.

Figure 7 illustrates the effect of convergence margin on the accuracy of the calculated coolant distribution. Generally, as the fineness of the mesh increases, the convergence margin must decrease in order to maintain accuracy. The convergence margin must also decrease with decreasing damping factor. For the 5 by 25 mesh and 0.3 damping factor of Figure 7, the solution has nearly converged for a margin of 0.0182. Convergence is complete at 0.005, although requiring twice the number of iterations.

Figure 8 illustrates the effect of the mesh dimensions on the predicted coolant distribution. The nosetip geometry and multidimensional flow are handled adequately by even a very coarse mesh. It should be noted, however, that these solutions ignore temperature effects. Due to the coupling between the pressure and temperature fields through fluid viscosity, fine partitioning in the radial direction is desired for accuracy.

Angle-of-Attack Effects

Figure 9 presents the coolant distribution at the nosetip surface for 20-deg angle of attack at high stagnation pressure. As is evident, there is substantial cross flow from the windward meridian toward the leeward meridian. It is clear that axisymmetric analyses using only the windward meridian pressure distribution would provide misleading results.

Figure 10 presents windward meridian coolant distribution for various angles of attack. The turbulent heating distribution on a hemisphere usually peaks around 30 deg from the stagnation point. In view of the altered coolant distribution at high angle of attack, substantial increases in coolant supply pressure will be required to provide adequate coolant flux as the heating profile shifts over the nosetip surface.

Comparison with Two-Dimensional Approximation

Figure 11 presents a comparison of the results obtained at two pressure levels using the present method with the method of Timmer and Dirling, [4] who approximated inertial effects and truncated their flow distribution at the tangency point. At the high-pressure, high-flow condition, the present solution is consistently lower. This is because Timmer and Dirling approximated the quantity $(\alpha\mu + \beta\rho v)$ as a constant in their solution by setting the velocity component equal to the average coolant velocity at the nosetip outer surface. This underestimates inertial effects, thus providing higher fluxes. The Timmer and Dirling solution also does not have the upward trend at the tangency point. This is due to the truncated solution. The solution at the lower pressure level appears to agree fairly well.

Temperature Effects

The results presented are for isothermal porous flow using the supply temperature of the coolant. Figure 12 shows how isothermal results compare with solutions coupling the porous flow enthalpy and pressure fields while accounting for heat conduction and viscous dissipation, and the partially coupled solution allowing only for viscous dissipation in the coolant.

At the high-pressure level, the isothermal solution provides slightly lower fluxes while the viscous dissipation approximation

agrees very well with the completely coupled solution. The reason for the good agreement is that the high coolant flux causes steep temperature gradients near the outer surface, essentially isolating the main portion of the porous flow from substantial heat conduction. The viscous dissipation solution predicts even slightly higher flows in the stagnation region, although this is due to greater streamline curvature for the fully coupled solution.

For the lower pressure level, the fully coupled solution provides substantially higher coolant fluxes than the isothermal or viscous dissipation approximations. This is because heat conduction has a greater effect on in-depth temperatures in the porous flow; as indicated by Equation (9), the temperature gradient along the porous flow vector should be proportional to coolant flux. The isothermal and viscous dissipation solutions coincide almost exactly, as very little flow work is done on the coolant.

Therefore, if accurate porous flow estimates are required over a wide range of reentry conditions, the fully coupled solution which accounts for both heat conduction and viscous dissipation through the porous flow energy equation should be utilized.

CONCLUSIONS

The conclusions are:

1. A fully coupled three-dimensional porous flow solution can be obtained by simultaneously solving the pressure drop, mass continuity, and energy continuity equations in finite-difference form using iteration to relax the pressure and enthalpy fields.

2. The small pore size of typical porous material permits an energy model based on thermal equilibrium between the material and the coolant.

3. Damping is required to maintain stability in the computational procedure.

4. As the fineness of the nosetip mesh increases, the required amount of damping also increases.

5. Very coarse meshes can provide good accuracy, particularly for conditions where heat conduction is of secondary importance.

6. For high coolant fluxes, the importance of heat conduction is small and viscous dissipation dominates thermal effects on coolant distribution.

7. For low coolant fluxes, the importance of viscous dissipation is small and heat conduction dominates thermal effects on coolant distribution.

REFERENCES

1. Darcy, H., Les Fontaines Publiques de la Ville de Dijon, 1856.

2. Green, L., Jr., and P. Duwez, "Fluid Flow Through Porous Metals," Journal of Applied Mechanics, March 1951, pp. 39-45.

3. Schneider, P.J., and R.E. Maurer, "Coolant Starvation in a Transpiration-Cooled Hemispherical Shell," Journal of Spacecraft and Rockets, Vol. 5, No. 6, June 1968, pp. 751-752.

4. Timmer, H.G. and R.B. Dirling, Jr., "An Approximate Solution for the Flow of a Fluid Through a Porous Solid," AIAA Journal, Vol. 7. No. 2, Feb. 1969, pp. 371-372.

5. Hess, J.L., Extension of the Douglas Newmann Program for Axisymmetric Bodies to Include the Calculation of Potential, Nonuniform Cross Flow, Added Mass, and Conductor Problems, Report No. LB31765, Sept. 1, 1964, Douglas Aircraft Company.

6. Gold, H., R.E. Mascola, and P.C. Smith, Flow Characteristics of Porous Media and Surface Liquid Film Interactions, AIAA Paper No. 70-152, AIAA 8th Aerospace Sciences Meeting, New York, N.Y., Jan. 1970.

7. Curry, D.M., and J.E. Cox, Transient, Compressible Heat and Mass Transfer in Porous Media Using the Strongly Implicit Iteration Procedure, AIAA Paper No. 72-23, AIAA 10th Aerospace Sciences Meeting, San Diego, Calif., Jan. 1972.

8. Schuster, J.R., "Mass Loss From Thin Liquid-Surface Films Exposed to Re-Entry Heating and Shear," Journal of Spacecraft and Rockets, Vol. 9, No. 4, April 1972, pp. 271-276.

522-137 O - 73 - 36

Figure 1. Typical Transpiration-Cooled Nosetip

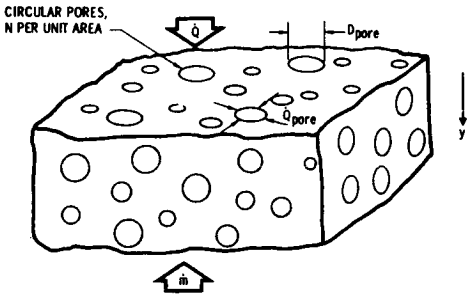

Figure 2. Idealized Porous Flow

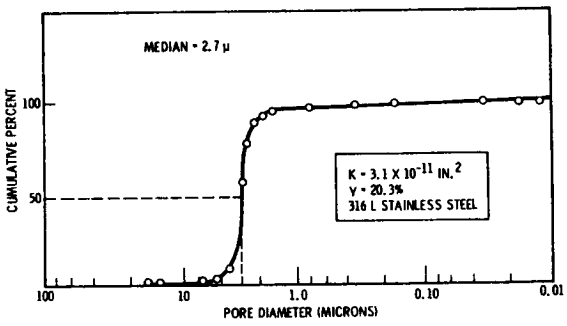

Figure 3. Typical Pore Size Distribution

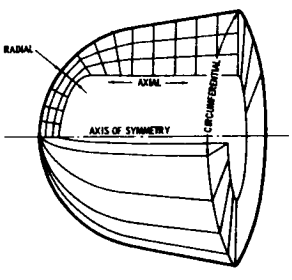

Figure 4. Nosetip Nodal Representation

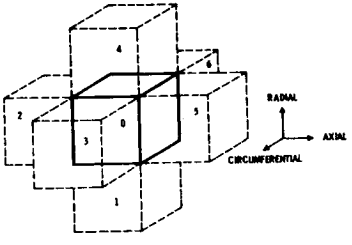

Figure 5. Nodal Matrix Numbering System

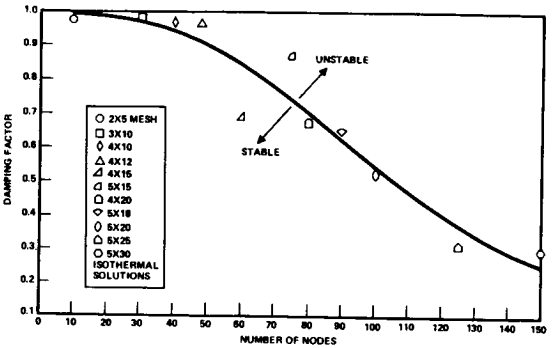

Figure 6. Damping Requirement for Convergence

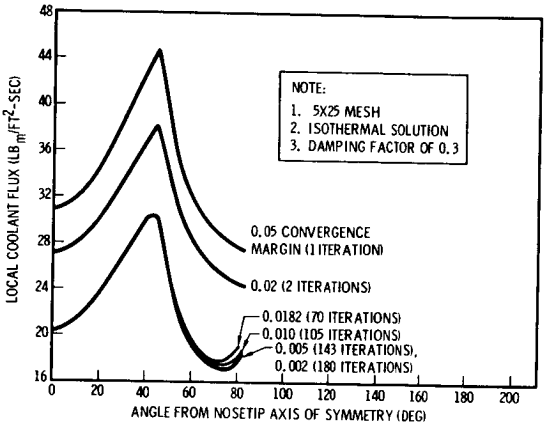

Figure 7. Effect of Nodal Convergence on Accuracy

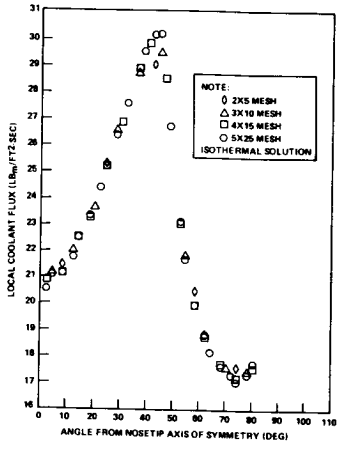

Figure 8. Effect of Mesh Fineness on Calculated Coolant Distribution

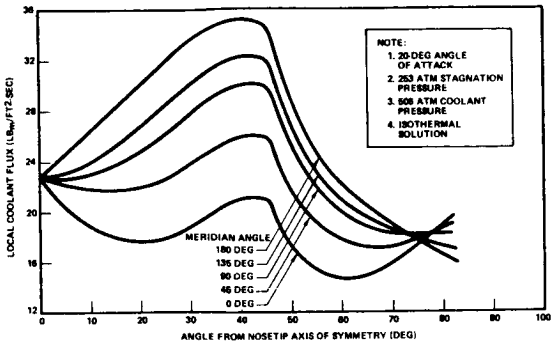

Figure 9. Nosetip Coolant Distribution at Angle of Attack

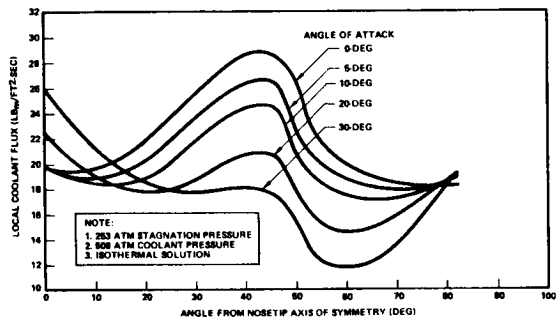

Figure 10. Effect of Angle of Attack on Windward Meridian Coolant Distribution

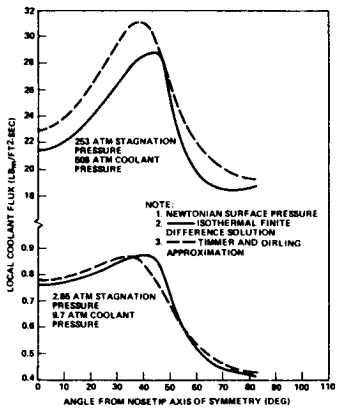

Figure 11. Comparison of Coolant Distributions

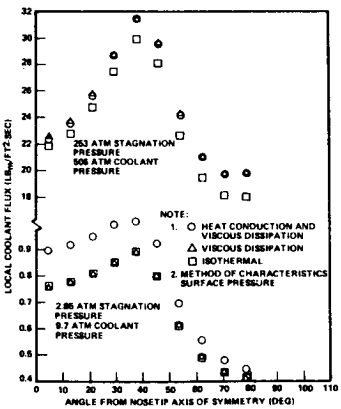

Figure 12. Effects of Energy Coupling on Coolant Flow Distribution